Proc. 13th Conference on Cloud Physics, Portland, OR, 28 June-2 July 2010, AMS, Boston, MA

JP3.17 IMPACT OF VARYING CCN CONCENTRATION ON THE PRECIPITATION PROCESS OF A SIMULATED CONVECTIVE STORM

Conrad L. Ziegler*[1], Edward R. Mansell[1], and Eric C. Bruning[2]

1. INTRODUCTION

The effects of the concentration of cloud condensation nuclei (CCN) on cloud microphysics have long been recognized (e.g., Pruppacher and Klett 1978). The potential impact of CCN on the precipitation process in convective storms is of great interest, since microphysics generally and particularly precipitation formation may strongly impact several areas of storm analysis and forecasting: for example, airflow dynamics, hydrology, electrification, chemistry, and their numerical predictions.

Precipitation in convective storms develops via some combination of warm- and cold-cloud processes (e.g., Fig. 1). The warm-cloud process is dominated by the combined effects of condensation with quasi-stochastic drop coalescence (i.e., binary coalescence or "self-collection" of cloud droplets to form drizzle-sized rain drops, followed by rain collection of cloud and rain "self-collection"). The cold-cloud process is initiated mainly by production of graupel embryos via: (1) drop freezing; and (2) vapor nucleation of crystals followed by riming of vapor-grown and aggregated snow particles. Subsequent precipitation growth is dominated by graupel riming of cloud. Rain is predominantly produced from graupel meltwater.

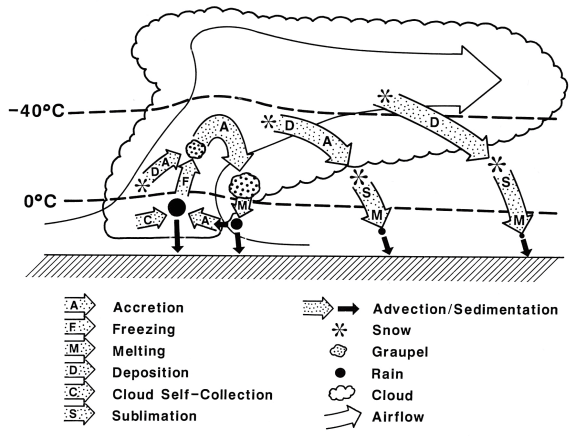

Figure 1: Conceptual diagram of precipitation processes in deep convective storms as derived from a 3D kinematic cloud model (adapted from Ziegler 1988).

The CCN concentration has the capacity to modulate the warm- and cold-cloud processes in several ways. For example, low (or alternatively, high) CCN forces the nucleation of low (high) concentrations of large (small) droplets, which in turn increase (decrease) the coalescence rate and accelerate (slow) the growth of rain drops. Graupel develop high (low) bulk densities and fallspeeds via riming of large (small) droplets. Frozen-drop graupel embryo formation is regulated by the median volume size of coalesced drops (which in turn is CCN-dependent) at temperatures at or colder than about - 5 to -10 °C.

The impact of CCN on convective storm evolution has been examined using numerical cloud models. For example, Li et al. (2008) implemented a two-moment bulk microphysics scheme in the WRF model, finding that precipitation in a simulated Texas Gulf coast storm increases with increasing CCN concentration from low to moderately high values due to suppression of warm rain coalescence and enhancement of the mixed phase precipitation process. Van Den Heever and Cotton (2007) demonstrated that simulated storm dynamics was sensitive to suppression of the warm rain process caused by CCN enhancement, thereby exerting a strong influence on precipitation by effectively modulating the time-integrated updraft vapor supply.

In the present study, the impact of varying CCN concentration of the parent airmass on the subsequent microphysical structure and evolution of a small, multicell storm is explored with a high-resolution, three-dimensional cloud model. The simulation is compared to a storm observed on 28-29 June 2004 during the TELEX experiment (Bruning et al. 2007).

2. CLOUD MODEL

a. Airflow dynamics

This study uses the Collaborative Model for Multiscale Atmospheric Simulation (COMMAS) (Wicker and Wilhelmson 1995). As described in Coniglio et al. (2006), the model uses the basic

*Corresponding author address: Dr. Conrad L. Ziegler, National Severe Storms Laboratory (NSSL), 120 David L. Boren Blvd, Norman, OK 73072; email: conrad.ziegler@noaa.gov
[1]NOAA/NSSL, Norman, Oklahoma
[2]Texas Tech University, Lubbock, Texas

equation set from Klemp and Wilhelmson (1978) which includes prognostic equations for momentum, pressure, potential temperature, and turbulent kinetic energy (Deardorff 1980). Time integration is performed with a third-order Runge-Kutta (RK) scheme (Wicker and Skamarock 2002). Advection on the first two RK iterations uses 5th-order upwind differencing. On the final RK step, scalar quantities (e.g., potential temperature, mixing ratio, number concentration, etc.) are advected using a sixth-order finite difference with a monotonicity filter (Leonard 1991) and are computationally diffused (horizontal directions only) with the simple monotonic filter of Xue (2000), following Bryan (2005). Wind components, on the other hand, are advected with a 5th-order weighted essentially non-oscillatory (WENO) scheme (Jiang and Shu 1996; Shu 2003). Sedimentation uses the Kato (1995) first-order box-Lagrangian scheme, with corrections for the two-moment system as in Mansell (2010) to prevent spuriously large particles and radar reflectivities.

b. Microphysics

The cloud model employs a detailed two-moment, bulk microphysical parameterization scheme which describes form and phase changes among a range of liquid and ice hydrometeors (Mansell et al. 2010). The two-moment microphysical parameterization predicts the mass mixing ratio and number concentration of cloud droplets, rain drops, cloud ice crystals, pristine and aggregated-rimed snow crystals, graupel, and hail. Hydrometeor size distributions are assumed to follow self-preserving, generalized-Gamma functional forms. Transfer rates between the vapor phase and the various hydrometeor categories are derived from governing equations for individual particles integrated over the appropriate hydrometeor size distribution. Microphysical processes include cloud droplet and cloud ice nucleation, condensation/deposition, evaporation/sublimation, collection-coalescence, variable-density riming, shedding, ice multiplication, cloud ice aggregation, freezing and melting, and conversions between hydrometeor categories.

CCN concentration is predicted as a single-category, monodisperse size spectrum approximating small aerosols. A subgrid parameterization of cloud droplet nucleation based on the work of Twomey is applied in cloud base updrafts that have achieved water supersaturation (Mansell et al. 2010). Further nucleation may occur higher in the updraft if water supersaturation exceeds the maximum diagnosed cloud base value.

The cloud model predicts the bulk graupel and hail particle densities as functions of rime layer density. Both the graupel and hail bulk densities are diagnosed by dividing predicted total mass by the predicted integral of particle volume over all sizes. Rime density in turn is a function of droplet size (e.g., affected by CCN concentration), impact speed, and ambient temperature. The graupel and hail particle densities are also used as roughness parameters to scale the drag coefficient in the expressions for particle fall speed.

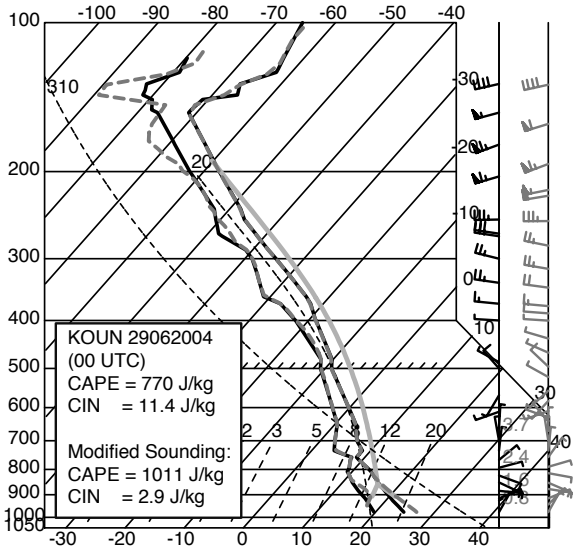

Figure 2: Modified model sounding (dashed gray curves) based on the operational sounding (solid black curves) from Norman, OK (OUN) at 00 UTC on 29 June 2004.

The prediction of hydrometeor number concentration is particularly critical to the resolution of secondary ice nucleation at higher temperatures (-5 < T < -20 °C) in the mixed phase updraft region, where ice crystals may be produced both by rime fracturing (Hallett–Mossop process) and by splintering of freezing drops in addition to a range of primary nucleation mechanisms.

c. Model domain, initialization, and integration

The horizontally-homogeneous model environment was initialized using a modified form of the National Weather Service (NWS) operational sounding at 00 UTC 29 June 2004 (Fig. 2). To improve consistency with available surface observations near the storm, the sounding modifications reduced the mixed layer convective inhibition (CIN) from 11.4 to 2.9 J kg^{-1} and increased CAPE from about 770 to 1011 J kg^{-1}. Simulations were performed in a 30-km by 30-km by 21.6-km domain with constant grid spacing of 250 m in the horizontal and 125 m in the vertical from the surface to 10 km, above which the grid spacing was stretched to a maximum of 500 m. The time step was 4 sec.

Vertical motion was initiated by applying a constant acceleration term to vertical velocity in the boundary layer (BL). The updraft nudging method is

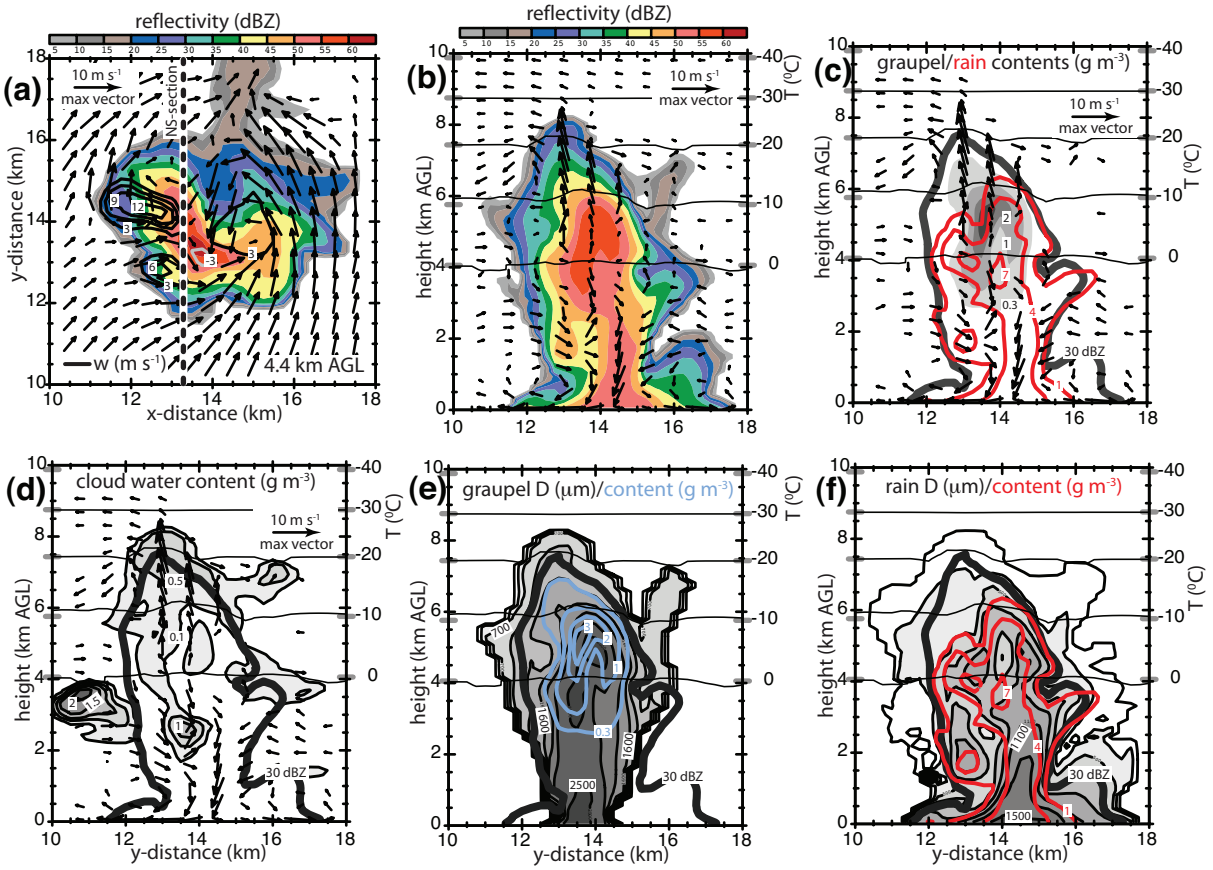

Figure 3: Cross-section at 51 min of the simulation using CCN concentration of 500 cm^{-3}. (a) Horizontal section of reflectivity with horizontal wind vectors and contours of vertical velocity (contour interval of 3 m s^{-1}). Panels (b-f) depict quantities in a S-N cross-section [indicated on (a)]. The heavy black contour in (c-f) is the 30 dBZ reflectivity outline. (b) Reflectivity and wind vectors. (c) Graupel content (0.3, 1, 2, 3 g m^{-3}) in gray-filled contours and rain content (1, 4, 7 g m^{-3}) in red. (d) Cloud water content (0.1, 0.5, 1, 1.5, 2 g m^{-3}). (e) Graupel mean volume diameter (400 to 2500 μm by 300 μm, gray filled) and graupel content as in (c). (f) Rain mean volume diameter (300 to 1500 μm by 200 μm, gray filled) and rain content as in (c).

consistent with roll-type mesoscale updraft forcing of convection initiation (e.g., Ziegler et al. 1997). Details of the updraft forcing term and random thermal perturbations can be found in Mansell et al. (2010).

A set of 17 simulations was run using the same initial conditions (and forcing) except for the base value of CCN concentration, which varied from 50 to 15,000 cm^{-3}. Initial CCN concentrations are assumed to be vertically well-mixed, and are therefore scaled by air density as $CCN(z) = CCN_{base}\,[\rho_{air}(z)/\rho_o]$.

3. RESULTS, DISCUSSION AND CONCLUSIONS

a. Mature storm morphology (CCN = 500 cm^{-3})

The model case with CCN = 500 cm^{-3} (similar to the control run of Mansell et al. 2010) illustrates the typical structure of the mature simulated storm near the time of peak overall precipitation and updraft intensity (Fig. 3). The initial updraft core in the storm, centered at (x,y) = (15 km,13.5 km), is decaying at 51 min, while two newer updraft cores are developing on the west flank of the main precipitation core (Fig. 3a). In a vertical south-to-north cross-section (Fig. 3b), the main precipitation core is downdraft-dominated below and updraft-dominated above 0 °C. Mixed-phase conditions combining millimetric graupel (Fig. 3c,e) with millimetric rain drops (Fig. 3c,f) and supercooled cloud droplets (Fig. 3d) increasingly characterize the sub-freezing updraft core region by around 51 min. Melting graupel and meltwater rain contents are equivalent via water substance conservation, although rain drops are smaller than graupel particles due to the initially moderate bulk densities of the melting graupel (e.g., CCN-dependent graupel density in Fig. 7b).

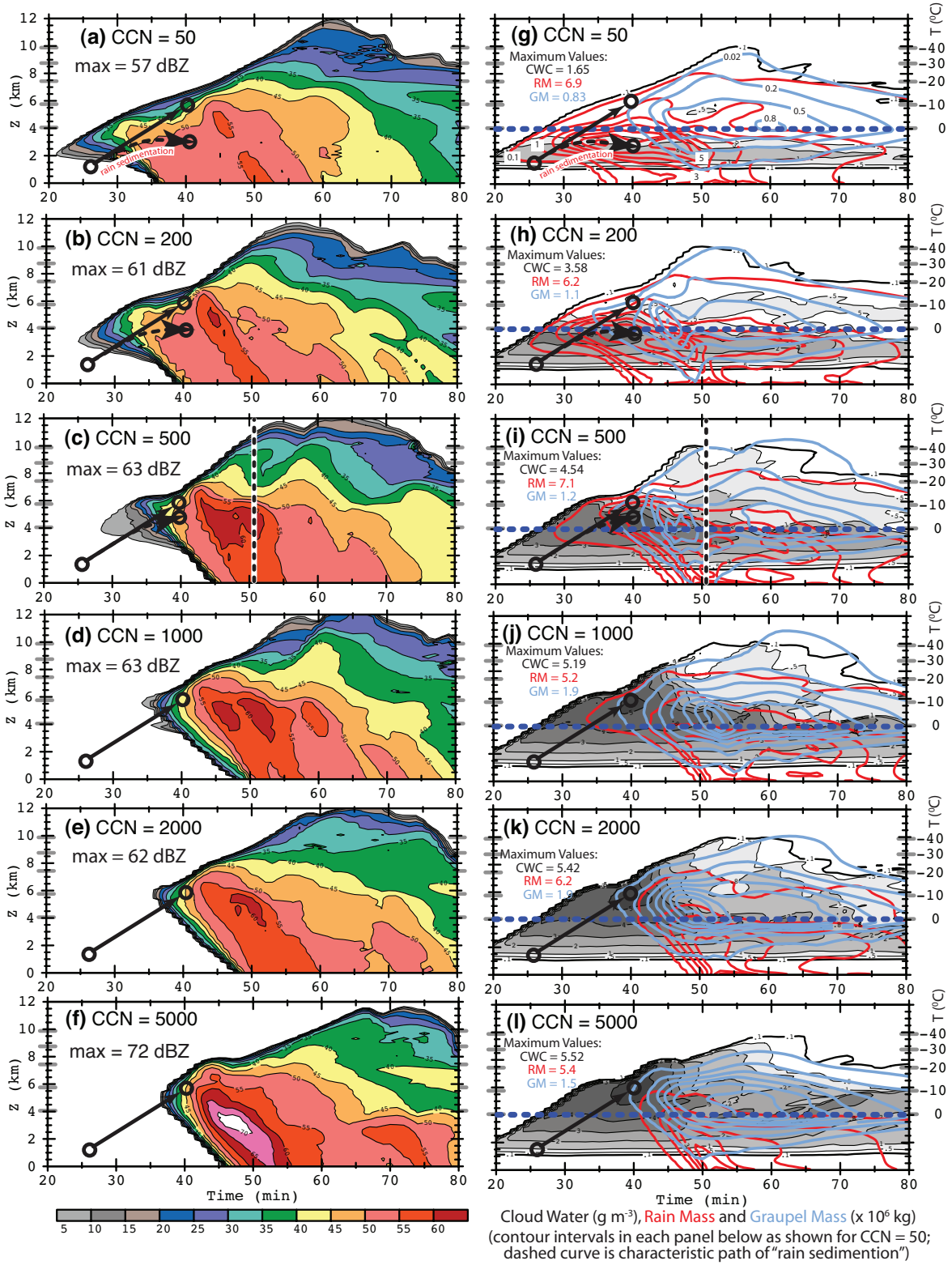

Figure 4: Time-height CCN dependence of: (a-f) maximum radar reflectivity; (g-l) maximum cloud water content (gray shading) and horizontally integrated rain (red contours) and graupel (blue contours) masses. In (f-j), the horizontal dashed line is the environmental 0C level. The vertical dashed line in (c,i) marks the time of the cross section plots in Fig. 3. Contour levels in (g-l) for graupel mass are 0.02 and >= 0.2 x 10^6 kg by intervals of 0.3, and for rain mass are 0.1, and >= 1 x 10^6 kg by intervals of 1. Solid arrows and dots represent a hypothetical adiabatic "bulk parcel" rising from cloud base to -10 °C in 14 min at 5 m s^{-1}, while dashed arrows and dots represent sedimentation of a peak-mass rain drop relative to the Lagrangian parcel.

Observations of the 28-29 June 2004 storm by NSSL's polarimetric radar (KOUN) revealed an updraft core that lifted raindrops above 0 °C, which subsequently froze and rimed to form moderate-density graupel particles (Bruning et al. 2007). The present model evidence is consistent with the earlier polarimetric radar analysis by inferring the presence of an active warm-rain mechanism of drop formation, with subsequent frozen-drop graupel embryo formation. Thus, a combination of warm- and cold-cloud precipitation processes are active in the 28-29 June storm for the case of CCN = 500 cm^{-3}.

b. Varying storm microphysical evolution with differing CCN

These model sensitivity tests include a range of ambient CCN concentrations (50 to 15,000 cm^{-3}) to control the mean droplet size at cloud base, thereby modulating drop growth via condensation-coalescence in low-CCN (e.g., "maritime-like") to extremely high CCN environments to represent anthropogenic aerosol effects (Fig. 4). The simulated time-height reflectivity, graupel mass, rain mass, and updraft volume all show systematic variations in their evolutions as the base CCN concentration increases.

Precipitation in the low-CCN simulated storm is stimulated by the formation of raindrops via stochastic collision-coalescence in regions of higher cloud water content (Fig. 4a). Increasing CCN concentrations reduce the collision-coalescence formation of drizzled-sized rain drops, which also shifts the initial reflectivity echoes to later times and higher altitudes (Fig. 4a-f). Drizzle-sized or larger raindrops lifted in updrafts begin freezing at temperatures around -10 °C to form graupel. Precipitation mass gradually becomes dominated by a graupel-based, cold-cloud riming process relative to the warm rain process (Fig. 4g-l).

As higher CCN concentrations increase the delay time for rain formation, drops appear at higher altitudes and lower temperatures (Fig. 4g-l) and have less time to accrete droplets before freezing. Even at the highest CCN concentrations, at least small amounts of drizzle-drops appeared before graupel due to sufficient updraft vapor supply for droplets to grow large enough via condensation to accelerate drop coalescence growth. The warm-cloud depth restricts ice crystal initiation to higher altitudes in the cloud, such that drop freezing appears to be the primary source of initial graupel in this case.

c. Varying storm dynamical evolution with differing CCN

The updraft volume enclosed by w > 5 m s^{-1} (Fig. 5) tends to show three maxima at increasing altitudes of 2-3 km, 6-7 km, and 8-11 km at times of about 25-30 min, 40-55 min and 55-65 min in the simulation. The updraft volume experiences similar

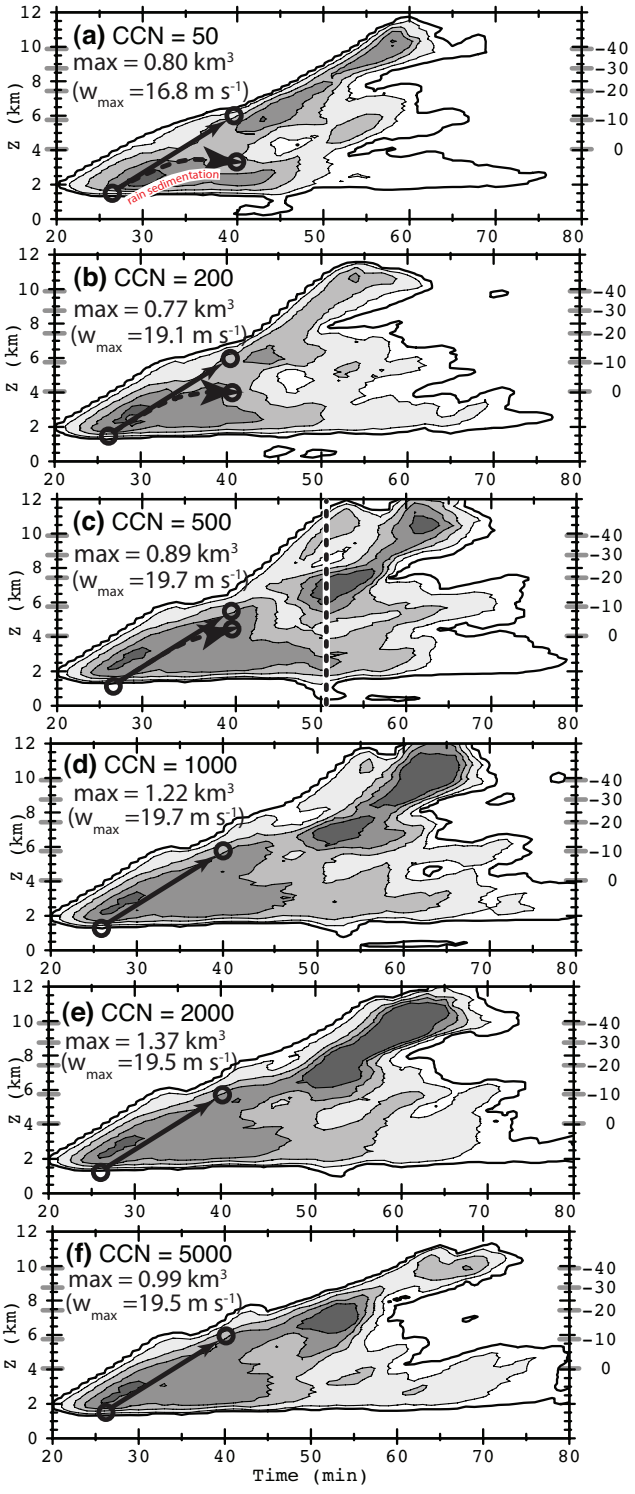

Figure 5: Time-height updraft volume where $w > 5$ m s^{-1}. Contour levels of 0.01, 0.1, 0.3, 0.5, 0.7 km^3. The vertical dashed line in (c) indicates the times of the plots in Fig. 3.

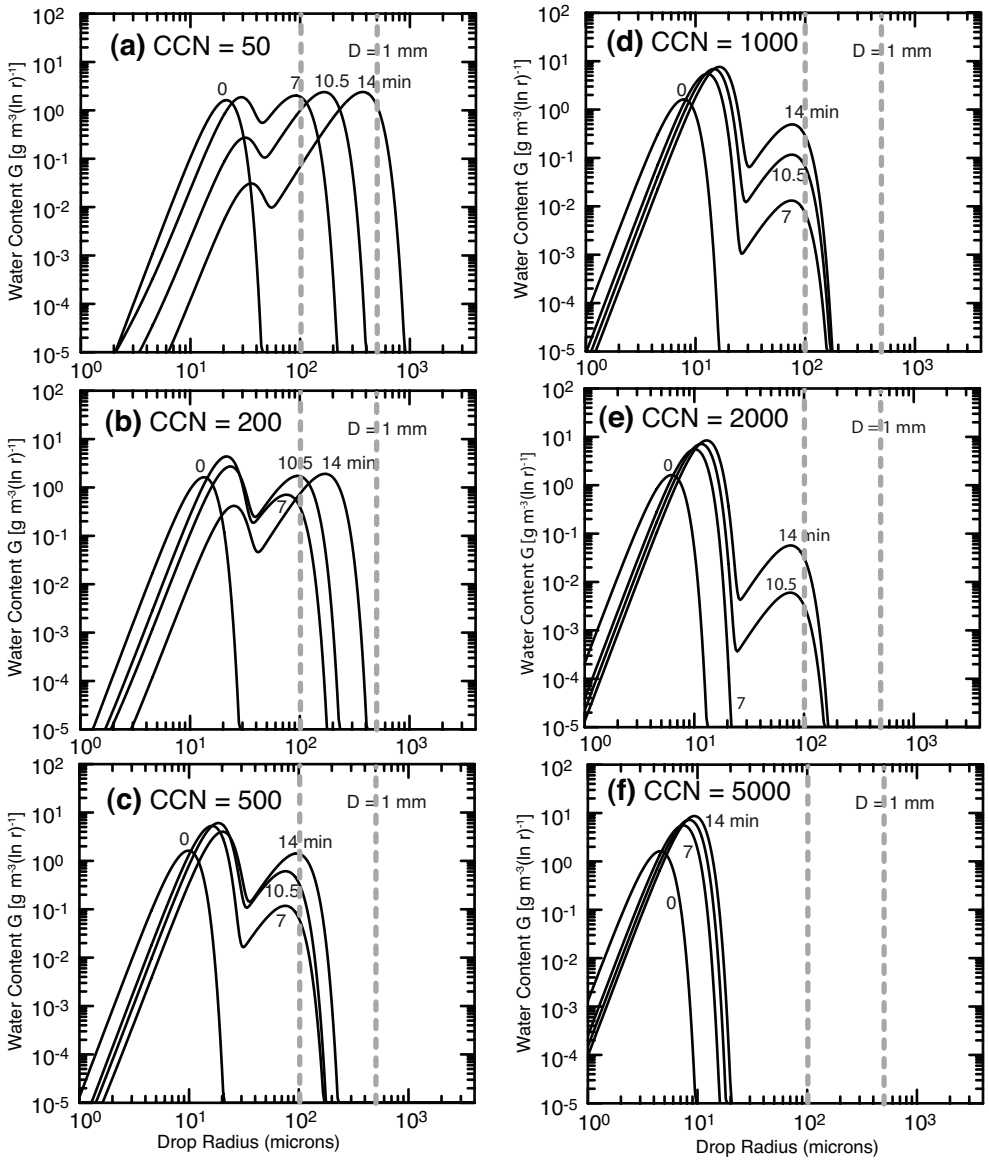

Figure 6: Drop spectra in a Lagrangian (no sedimentation) version of the warm-cloud physics used in COMMAS. For sake of simple illustration, an adiabatic "bulk parcel" is assumed to rise from cloud base to -10°C in 14 min at 5 m s^{-1} (with plotted spectra at 0, 7, 10.5, and 14 min). Condensation narrowing effects are not represented here, since the shape parameter is held fixed in the present 2-moment microphysics scheme (Mansell et al. 2010). Growth rates are large (small) at low (high) CCN.

evolution prior to precipitation formation for all CCN. At lower CCN values, increased loading with precipitation and reduced riming freezing (latent heating) at mid-levels leads to decreased updraft volume. Subsequent fallout and diabatic heating from ice formation forces a secondary updraft maximum above 6 km (-10 °C) for CCN > 500 cm^{-3}. Peak updraft values increase modestly with increasing CCN from 16.8 m s^{-1} (CCN = 50 cm^{-3}) to 19.5 m s^{-1} (CCN = 500 cm^{-3}). For CCN > 500 cm^{-3}, peak updraft varies little from 19.5 m s^{-1}.

The sensitivity of cold pool evolution to CCN is revealed by onset and decay of updraft volume in the lowest 1.5 km (Fig. 5). The onset of BL updrafts indicates the action of the solenoidal circulation at the margins of the cold pool (formed by rain evaporation). For example, the outflow-induced BL updrafts at 51 min in the CCN = 500 cm^{-3} run (e.g., Fig. 3b) are consistent with enhanced updraft volumes below 1.5 km at around 51 min (Fig. 5c). The onset of BL outflow-induced updrafts are delayed with increasing CCN in the range 50 - 1000

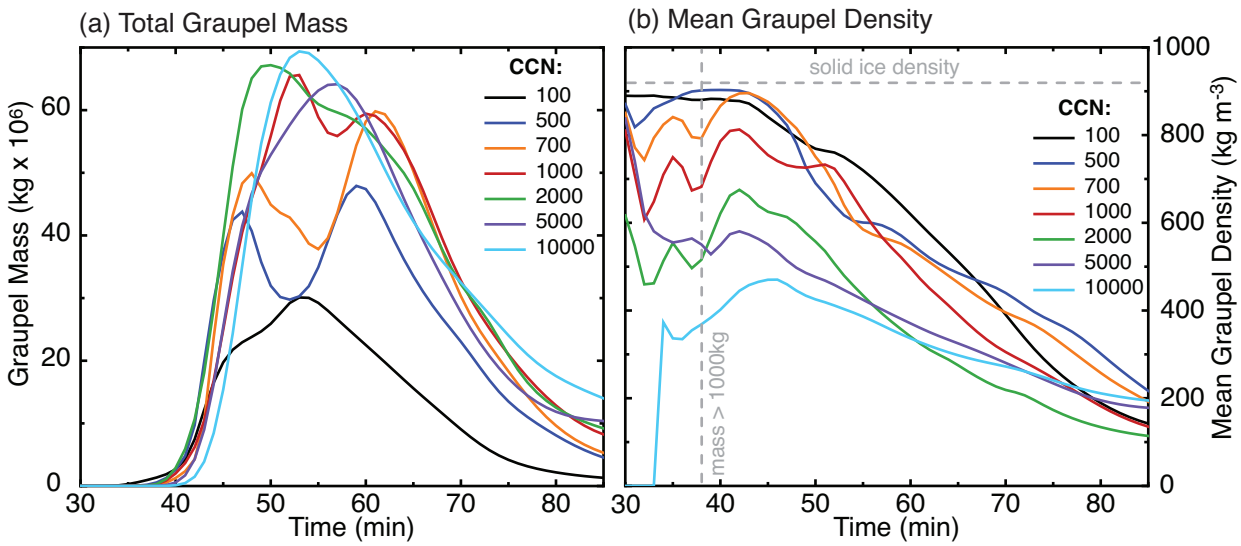

Figure 7: Time-series of (a) total graupel mass and (b) average graupel density. The vertical dashed line in (b) denotes the time at which all simulations have a total graupel mass of at least 1000 kg. Densities for $t < 38$ min may be biased by small total amounts of graupel, particularly for the higher CCN cases (5000 and 10,000 cm^{-3}).

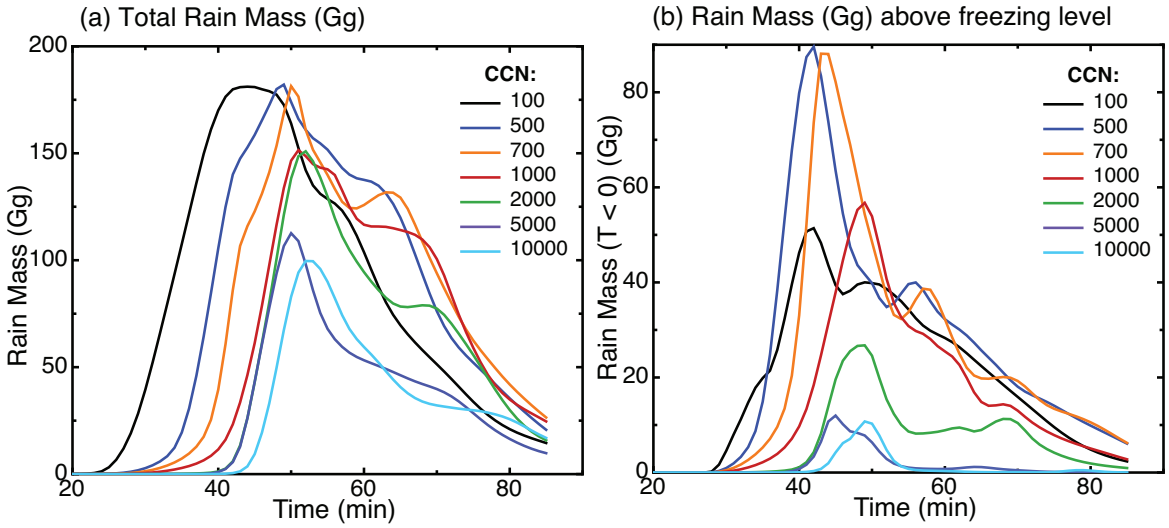

Figure 8: Time-series of (a) total rain mass and (b) rain mass above the 0°C isotherm for simulations with different base CCN concentrations.

cm^{-3} (Fig. 5a-d), consistent with the delayed onset of surface rainfall. The BL outflow-induced updrafts are significantly reduced for CCN exceeding 2000 cm^{-3} (Fig. 5e-f), implying that increasing rain drop sizes and fallspeeds coupled with decreasing concentrations via melting production from large (low-density) graupel particles is reducing bulk BL evaporation rates (not shown).

d. Sensitivity of the precipitation process to CCN

The prediction of cloud droplet and rain drop concentration and mass and their evolution proceeds through droplet vapor nucleation (i.e., via the modeled subgrid parameterization of peak cloud base supersaturation and concentration on CCN and updraft strength), condensation growth, and quasi-stochastic coalescence with subsequent vertical updraft transport above the freezing level. The drizzle-drops thus transported to altitude have sufficiently large volumes to force the production of graupel embryos via homogeneous drop freezing (i.e., Bigg freezing), as previously shown by Ziegler (1988), with additional drop freezing occurring in the present model via crystal contact nucleation.

A Lagrangian parcel model previously employed to test the two-moment warm rain parameterization

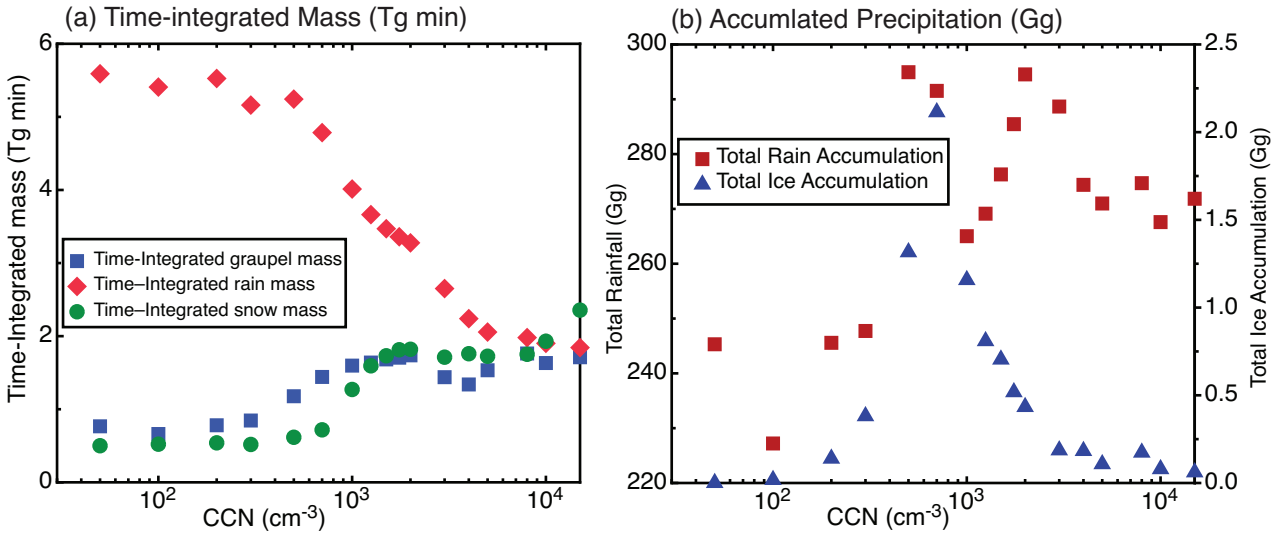

Figure 9: (a) Time integrated rain, graupel, and snow masses. (b) Total domain accumulated rain and ice.

(Ziegler 1985) has been updated to include condensation, providing a simple illustration of the effects of increasing CCN concentration on coalescence growth in the simulated storm (Fig. 6). The Lagrangian model assumes an adiabatic "bulk parcel" that rises from cloud base to -10°C in 14 min at 5 m s^{-1}. Condensation growth of droplets following the motion increases the collection kernel and thus accelerates binary coalescence rates in the updraft (e.g., as previously shown by Leighton and Rogers 1974). In opposition to the acceleration of coalescence by condensation, increasing CCN simultaneously decreases median droplet size and increases total concentration. The resultant net drop spectral growth rates are large (small) at low (high) CCN (Fig. 6).

e. Graupel mass and bulk density vs. time and CCN

The peak values of domain-integrated graupel mass (Fig. 7a) tend to increase monotonically with CCN, with maximum values occurring in the multicell storm core at ~ 50-60 min (e.g., also refer to Fig. 3 for case of CCN = 500 cm^{-3}). Conversely, the domain-averaged bulk graupel density (Fig. 7b) tends to decrease with increasing CCN due to smaller droplet sizes and lower graupel fall speeds (i.e., relative to a reference graupel size) in the rime layer density parameterization employed by COMMAS.

f. Precipitation mass vs. CCN

Comparing the evolutions of the integrated rain mass volumes of the storm (Fig. 8a) and the sub-freezing region (Fig. 8b), increasing CCN in the ~100-700 cm^{-3} range both delays and elevates the region of rain formation by coalescence. Further increasing CCN to >> 1000 cm^{-3} reduces and (for CCN > 5000 cm^{-3}) sharply reduces elevated rain formation, a result that is also consistent with the increasing dominance of meltwater rain formation. At extreme values of CCN > 5000 cm^{-3}, the relatively few drops that form from binary coalescence are lofted to colder temperatures where they quickly freeze.

The time-integrated ratio of storm-total rain to graupel masses (e.g., Fig. 9a) decreases to ~1 with increasing CCN approaching 5000 cm^{-3}, illustrating the increasing dominance of graupel meltwater for the production of rain with increasing CCN. The time-integrated, storm-total snow crystal mass increases as graupel mass with increasing CCN, indicating increased crystal mass growth via riming and deposition in the higher cloud water contents and diabatically-warmed (and, hence, more ice-supersaturated) conditions in the updraft core.

The total accumulated surface rainfall (Fig. 9b) increases by ~ 20% from ~ 100 cm^{-3} to ~ 1000 cm^{-3} due to the combined effects of larger drops and graupel, higher fall speeds, and reduced sub-cloud evaporation. Localized peak rainfall increases of up to 26% are obtained at ~ 500 cm^{-3} and ~ 2000 cm^{-3}, suggesting that bulk rainfall may be somewhat sensitive to initial conditions or other external factors that influence the storms' dynamical evolutions. The product of increasing graupel mass with decreasing graupel fall speed (i.e., from decreasing bulk density) causes graupel precipitation to maximize at ~ 700 cm^{-3} (Fig. 9b).

g. Impact of CCN on storm electrification

As a byproduct of the variation of simulated cloud and precipitation content with CCN, additional cloud simulations in which optional electrification mechanisms were activated in COMMAS manifest a sensitivity of microphysical charge separation and

lightning production to CCN changes (Mansell et al. 2010). Similar rates of simulated and observed intracloud (IC) and cloud-to-ground (CG) flashes and CG polarities were obtained for the 28-29 June 2004 storm in the model simulation case that assumed an ambient CCN value of ~ 400 cm^{-3}.

The maintenance of sufficiently large rates of rebounding collisions between graupel and ice crystals in the presence of supercooled cloud water in a convective updraft is conducive to strong electrification, in turn forcing lightning discharges. Thus, the joint internal consistency of the COMMAS model predictions of microphysical and electrical characteristics and their broad agreement with independent radar and lightning mapping array (LMA) observations increases confidence in the storm simulations while emphasizing the importance of CCN as an important modulator of the precipitation process in storms.

4. ACKNOWLEDGEMENTS

Support for the present research was provided by the National Severe Storms Laboratory. Partial funding for this research was also provided by NSF grant ATM-0451639. Some of the computing for this project was performed at the OU Supercomputing Center for Education & Research (OSCER) at the University of Oklahoma (OU).

5. REFERENCES

Bruning, E. C., W. D. Rust, T. J. Schuur, D. R. MacGorman, P. R. Krehbiel, and W. Rison, 2007: Electrical and polarimetric radar observations of a multicell storm in TELEX. *Mon. Wea. Rev.*, **135**, 2525–2544, doi:10.1175/MWR3421.1.

Bryan, G. H., 2005: Spurious convective organization in simulated squall lines owing to moist absolutely unstable layers. *Mon. Wea. Rev.*, **133**, 1978–1997.

Coniglio, M. C., D. J. Stensrud, and L. J. Wicker, 2006: Effects of upper-level shear on the structure and maintenance of strong quasi-linear mesoscale convective systems. *J. Atmos. Sci.*, **63**, 1231–1252.

Deardorff, J. W., 1980: Stratocumulus-capped mixed layers derived from a three-dimensional model. *Bound.-Layer Meteor.*, **18**, 495–527.

Jiang, G.-S. and C.-W. Shu, 1996: Efficient implementation of weighted ENO schemes. *J. Comp. Phys.*, **126**, 202–228.

Kato, T., 1995: A box-Lagrangian rain-drop scheme. *J. Met. Soc. Japan*, **73**, 241–245.

Klemp, J. B. and R. B. Wilhelmson, 1978: The simulations of three-dimensional convective storm dynamics. *J. Atmos. Sci.*, **35**, 1070–1096.

Leighton, H. G., and R. R. Rogers, 1974: Droplet growth by condensation and coalescence in a strong updraft. *J. Atmos. Sci.*, **31**, 271-279.

Li, G., Y. Wang, and R. Zhang, 2008: Implementation of a two-moment bulk microphysics scheme in the WRF model to investigate aerosol-cloud interaction. *J. Geophys. Res.*, **113**, 21 pp., doi: 10.1029/2007JD009361.

Leonard, B. P., 1991: The ULTIMATE conservative difference scheme applied to unsteady one-dimensional advection. *Comp. Methods Appl. Mech. Eng.*, **88**, 17–74.

Mansell, E. R., C. L. Ziegler, and E. C. Bruning, 2010, Simulated electrification of a small thunderstorm with two-moment bulk microphysics. *J. Atmos. Sci.*, **67**, 171-194.

Mansell, E. R., 2010, On sedimentation and advection in multi-moment bulk microphysics, *J. Atmos. Sci.,* **67**, [In press].

Pruppacher, H. R., and J. D. Klett, 1978: *Microphysics of clouds and precipitation*. D. Reidel, 714 pp.

Shu, C.-W., 2003: High-order finite difference and finite volume WENO schemes and discontinuous Galerkin methods for CFD. *Int. J. Comp. Fluid Dyn.*, **17**, 107–118.

Van Den Heever, S. C., and W. R. Cotton, 2007: Urban aerosol impacts on downwind convective storms. *J. Appl. Meteor. Clim.*, **46**, 828-850, doi: 10.1175/JAM2492.1

Wicker, L. J. and W. C. Skamarock, 2002: Time-splitting methods for elastic models using forward time schemes. *Mon. Wea. Rev.*, **130**, 2088–2097.

Wicker, L. J. and R. B. Wilhelmson, 1995: Simulation and analaysis of tornado development and decay within a three-dimensional supercell thunderstorm. *J. Atmos. Sci.*, **52**, 2675– 2703.

Xue, M., 2000: High-order monotonic numerical diffusion and smoothing. *Mon. Wea. Rev.*, **128**, 2853–2864.

Ziegler, C. L., 1985: Retrieval of thermal and microphysical variables in observed convective

storms. Part I: Model development and preliminary testing. *J. Atmos. Sci.*, **42**, 1487–1509.

_____, 1988: Retrieval of thermal and microphysical variables in observed convective storms. Part II: Sensitivity of cloud processes to variation of the microphysical parameterization. *J. Atmos. Sci.*, **45**, 1072–1090.

_____, T. J. Lee, and Roger A. Pielke, Sr., 1997: Convective initiation at the dryline: A modeling study. *Mon. Wea. Rev.*, **125**, 1001–1026.